Int. J. Rock Mech. Min. Sci. & Geomech. Abstr. Vol. 27, No. 5, pp. 329–343, 1990
Printed in Great Britain.

0148-9062/90 $3.00 + 0.00

Joint Roughness Measurement Using Shadow Profilometry

N. H. MAERZ†
J. A. FRANKLIN†
C. P. BENNETT‡

The shadow cast by a ruler or string reveals a roughness profile across a joint surface. If the rock is smooth, the edge of the shadow is straight, and if rough, the shadow is irregular. The image can be recorded on video tape, digitized by an image analyzing microcomputer, then processed to isolate the shadow edge. Parameters of roughness can then be calculated and displayed.

This photoanalysis method compares favourably with the often awkward and impractical mechanical and optical techniques of roughness measurement. In a series of laboratory and field experiments, the authors have investigated errors resulting from variations of illumination and image processing. Results demonstrate that with reasonable precautions, the results can be reproduced to within about 5% of the full roughness range.

Roughness parameters convey in a quantitative manner the meaning of "smooth" and "rough", and are needed as a basis for prediction of shear strength and other properties. The many available alternative parameters, borrowed from fields of electronics, acoustics and mechanical engineering, range from simple measures of amplitude, wavelength and slope, to more complex stochastic, frequency domain and fractal anaylses. These are reviewed, and criteria for selection discussed.

Shear strength models based on roughness include those of Patton, Ladanyi and Archambault, and Barton. Barton's JRC is not a geometric property: it must be estimated either from shear tests or by comparing a rough joint with the published standard set of comparator profiles. Visual comparison is found to be unreliable. Better results can be obtained by digitizing the standard profiles using the method described in this paper, and relating JRC to a measurable quantity, the roughness profile index, R_p. The regression equation relating JRC to R_p compares closely with the same form of equation determined by direct correlation of the results of shear testing and roughness measurement.

INTRODUCTION

Measurements of jointing using tape measures, geological compasses and profilographs are slow, and often lead to engineering designs based on statistically inadequate samples of the data.

Photoanalysis techniques provide a more practical alternative [1–3]. Images of the rock are digitized from still photographs or video tape, then enhanced to measure roughness, orientation, spacing and trace length. A quick survey of a mine by video camera can record much of the information on jointing needed for rock mass classification and analysis of stability. The same method can quantify the results of blasting, including characteristics of overbreak and fragmentation.

Measurement of roughness is the focus of this paper. If roughness can be measured reliably, characteristics such as shear strength [4–6] rock mass deformability [7–9] and hydraulic conductivity [10, 11] can be predicted for use in design.

TRADITIONAL METHODS OF MEASUREMENT

Mechanical methods

Measurements of roughness are well-established in mechanical engineering, particularly at microscopic scales, and include contacting methods, taper sectioning and optical techniques [12–14].

Among the contacting methods, mechanical or electronic stylus profilometers give precise measurements along a traverse. Deflection of the stylus is recorded as a function of position. Less direct contacting methods

†University of Waterloo, Ontario, Canada.
‡Shell Oil, Calgary, Alberta, Canada.

include tactile tests, measurements of kinetic or static friction using a rolling ball (similar to the tilt test of Barton and Choubey [15]), and measurements of the compliance of a metal sphere with a rough surface [14]. On a larger scale in civil engineering, the roughness of a road surface is measured dynamically using a vertical accelerometer [16]. Taper sectioning, a method of metallurgy, consists of cutting across a surface at a low angle α to physically amplify the height of asperities by cot α [14].

Optical methods

Optical methods include light section microscopy, interferometry, speckle metrology and laser profilometry.

Light section microscopy [17] illuminates a rough surface with a thin slit of light at an angle of 45°. The surface is observed at 90° from the direction of illumination. The projected slit appears as a straight line if the surface is flat, and as a progressively more undulating line as the roughness of the surface increases.

Interferometry [12] and speckle interferometry [18] use the interference fringes produced when monochromatic and laser light are reflected off a rough surface and a flat reference surface. The fringes are contours of roughness at a contour interval of about one-half the wavelength of the light used. The technique thus can be used only for quite smooth surfaces.

On a larger scale, ocean wave profiles have been measured by reflecting laser light off the surface of the water [19].

Measurements in rock mechanics

ISRM Suggested Methods for the Quantitative Description of Discontinuities in Rock Masses [20] include three techniques for measuring joint roughness, namely profilometry [21, 22], compass and disc clinometry [21] and photogrammetry [23].

Profilometry can be a manual measurement of the distance between a reference line and the rock, or an electrical one, with the help of a transducer. Delicate apparatus has to be mounted on the joint surface, and much time is often spent at difficult and dangerous locations. Roughness measurements on plastic replicas of the rock surface may be safer, but are usually less convenient.

As an alternative, Barton and Choubey [15] recommend estimating roughness by visually comparing rock joints with a series of 10 standard profiles of known roughness, a method investigated and discussed later in this paper. The roughness profiles are classified in terms of JRC (joint roughness coefficient) which is actually a measure of shear strength, not of the geometry of roughness directly.

THE SHADOW PROFILE TECHNIQUE

Measuring principle

The intersection of a plane with a 3-D rough surface produces an irregular line whose waveform is a linear (2-D) measure of roughness. When the intersection is at right angles, the *roughness waveform* becomes a true *roughness profile*, i.e. a cross-section through the surface.

In the taper sectioning method outlined above, actual physical slicing produces a waveform. A low angle of cut amplifies the roughness as an aid to measurement. Similar amplification can be achieved using the Schmaltz microscope method also outlined above, but here the planar "cut" is provided by a narrow slit of light without physically slicing the surface.

In the method of shadow profilometry, a planar intersection is provided by the edge of a shadow cast onto the rock surface from a straightedge. If the rock is smooth, the shadow edge is straight, and if rough, the shadow is irregular. Figure 1 gives a simple illustration using a piece of corrugated cardboard.

With illumination at 45° to the surface, the height of the shadow is the same as the height of the asperity. With other angles of illumination, the true asperity height is magnified or diminished, and a correction factor must be applied if a true roughness profile is to be obtained from measurements on the shadow waveform. Angle of illumination is calculated from the length of shadow cast by a "shadow post" of known height, as shown in Figs 1, 2 and 6.

Source of illumination

The portable equipment required to record roughness in the field includes a light source, a straightedge shadow bar, and a video camera (Fig. 2).

The sharp shadow needed for precise measurement is obtained, ideally, with a point source of light. Real sources have a finite size and tend to give a blurred shadow unless they are both bright and distant. In practice, the light should be as small, as bright, and as far from the surface as possible. If the lighting is diffuse, the shadow can be sharpened by placing the straightedge closer to the rough surface.

For video camera field work, brilliant illumination is provided by a portable battery-powered spotlight. The authors are using a General Electric Q4554 PAR 46, 28 V 450 W quartz–halogen aircraft landing/taxiing lamp, whose parabolic reflector has a 50° horizontal and 11° vertical spread. The lamp is powered by a Concorde CB-24-11M lightweight, 24 V, 17 AH vented lead–acid aviation battery.

The single lamp gives an intensity of illumination that fades towards the edges of the image. The image analysis software described below compensates for uneven lighting, but even then, the usable zone of illumination is limited to about a 3 m radius, sufficient in most applications.

For still camera work, an electronic flash gives a small and brilliant source during the short interval of film exposure, and is lightweight and convenient. A supplementary, continuous and low-intensity light should be mounted alongside the flash to permit focussing of the camera and adjustment of the angle of illumination.

When available, sunlight gives sharp shadows and a uniformity of illumination that is hard to match with

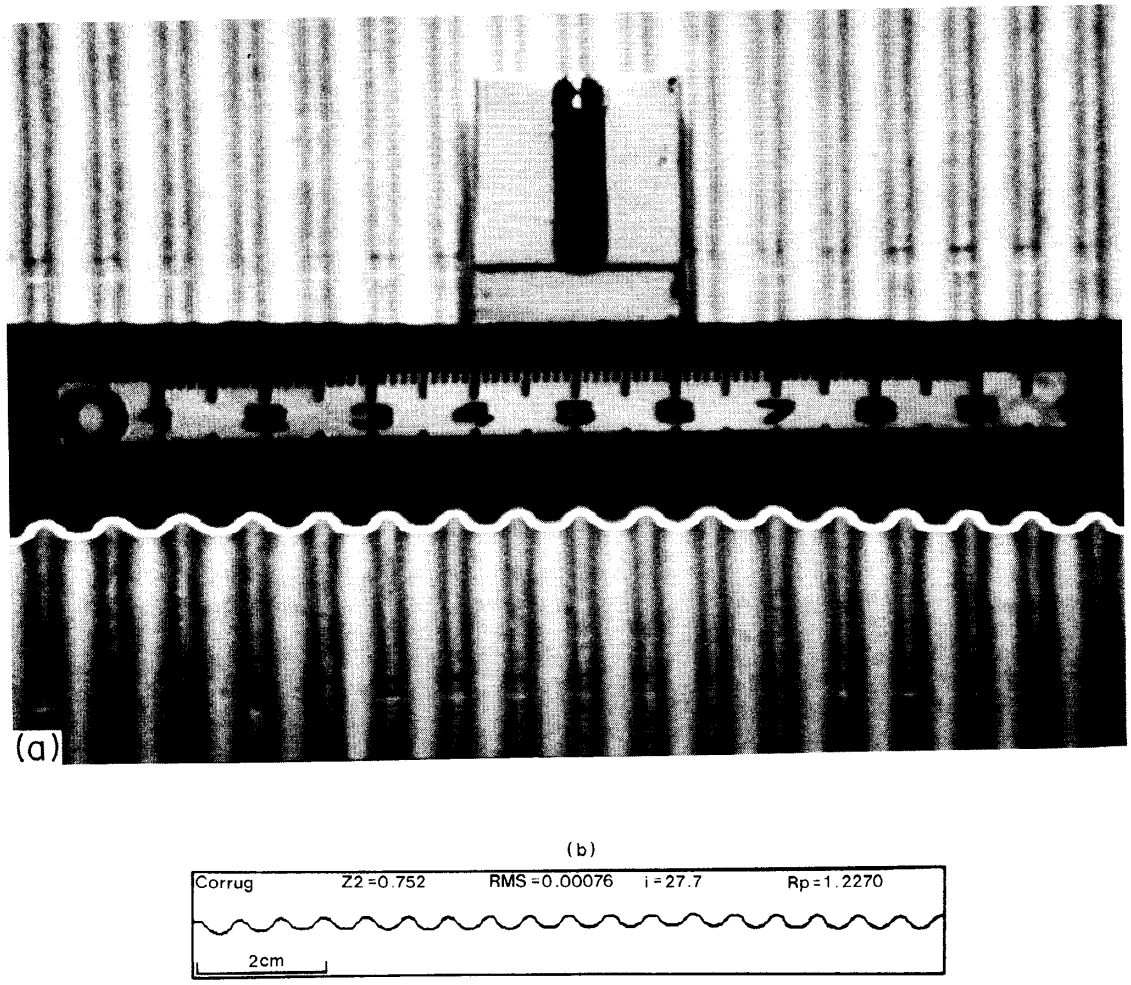

Fig. 1. Image analyis—example using corrugated cardboard: (a) isolated shadow edge (appears in colour on screen) superimposed on the black–white enhanced original; and (b) corrected profile with analytical results for Z_2, RMS, i, and R_p roughness parameters.

close-up artificial lighting. Unfortunately, sunlight tends to be unreliable, is diffused by cloud cover, and the angle of illumination cannot be adjusted.

Straightedge and sundial

Using a sundial with a shadow post of known height in the picture, the length of shadow gives the angle of incidence of the lighting, and the sundial's diameter or the length of the straightedge gives the scale. The sundial face should be white to contrast with the shadow, and can be marked with circles to help set the correct angles of illumination.

For sampling lengths no greater than about 1 m, a straightedge of the type shown in Fig. 1 with integral shadow post is convenient. Greater lengths require a surveyor's tape, stretched string or longer rigid straightedge with separate sundial in the field of view, as shown in Fig. 2. Straightness and closeness of the string or tape to the surface of measurement are sometimes difficult to ensure.

Camera

A highly sensitive camera allows measurements over a greater part of the illuminated area, reduces the requirement for brilliant lighting and heavy batteries, and makes the equipment as a whole more portable.

The authors use a Panasonic Omnivision PV-S350-k video camcorder (camera and recorder), with 400 lines of resolution and with NTSC video output. Minimum illumination is 1 lx. The storage medium is S-VHS video tape.

Alternatively, the image can be stored on photographic film, with the benefit of flash lighting. Still cameras give greater resolution, but this advantage is lost when the photograph is later digitized by a video camera in the laboratory. Use of a video camera in the

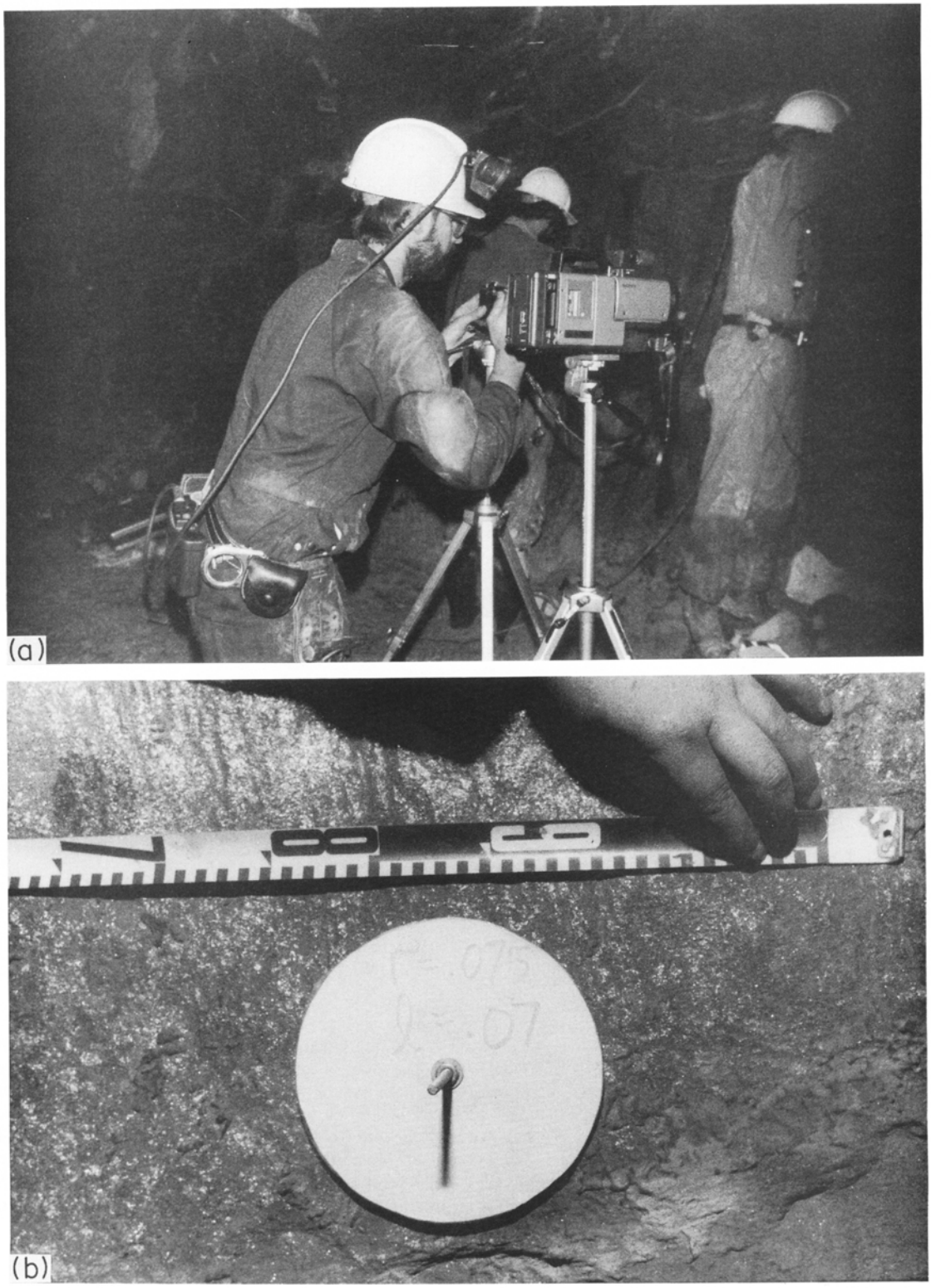

Fig. 2. Equipment for taking roughness measurements: (a) video camera and high-intensity lighting underground at Noranda's Hemlo Mine; and (b) surveyor's tape used as a straightedge alongside a "sundial" type of shadow post.

field eliminates this double-handling and deterioration of the image, saves time and expense in photographic processing, and allows the user to select an image from many frames stored in compact video tape format.

Image analysis hardware

The analogue image from video tape, or from a video camera scanning a still photograph, must be converted to a digital image using an appropriate "frame grabber" (digitizer). The authors use a PCVISIONplus frame grabber and image display buffer, which has a resolution of 512 × 512 × 256. The frame buffer resides in a microcomputer with either 80286/7 or 80386/7 processors and numerical coprocessors. Graphical output is provided by an EGA/VGA adapter and the PCVISIONplus frame buffer.

PROCEDURE

Sampling the joint system

The joint system at any given location consists of a population of joints that may cluster into subparallel sets. Joint roughness estimation calls for three levels of sampling: selection of representative joints, selection of a sampling line and selection of points along the line. The first two are at the discretion of the engineer, whereas the last level of sampling is controlled by the hardware that scans the recorded image.

Sampling of joints must take into account that different sets are quite likely to have different roughnesses, and that roughness may also vary within a single set at different locations. For example, some beds in a sedimentary rock may be sheared and slickensided, and others separated along micaceous or shaly partings. These variations in roughness are reflected by a spectrum of shear stengths. The size of sample, i.e. the number, positions and directions of profiles, depends on the required accuracy and reliability. Access is often difficult. Serious sampling biases can result from sampling only where convenient.

The direction of the sampling line needs to be varied in a systematic or random manner taking into account the possibility of anisotropic roughnesses such as those of ripple-marked beds or plumose tension joints. If a scale effect is present, sample images are also needed at different scales of observation.

Availability of a simple and quick measuring technique makes it possible to investigate each of these effects, and to determine the appropriate sampling frequencies, locations and directions.

Angles of camera and lighting

The camera should be aimed at right-angles to the rock surface. However, the measurements are not very sensitive to this perpendicularity, and an error of 5° gives an error of less than 1% in the roughness measurements.

A 45 ± 5° angle of illumination is recommended when feasible. Errors caused by incorrect measurement of this angle are then at a minimum. High angles of illumination give short shadows, hence poor accuracy. Low angles give greater accuracy, but at very low angles, the shadows cast by asperities tend to interfere with the shadow cast by the straightedge.

Sampling the recorded image

Digitizing an image requires sampling at predetermined intervals in a 2-D grid. The vertical sampling interval is set by the spacing of video scanlines. The horizontal scanline, being a continuous analogue signal, can be sampled at various rates, limited only by the bandwidth of the signal. Typically a horizontal resolution of 1/256, 1/512 or 1/1024 of the image width is used by digitizers.

A profile should fill the screen: using the author's digitizer, a 100 mm profile occupies most of a 512 pixel-wide image, giving a sampling interval of 0.2 mm. A 10 m profile has a sampling interval of 20 mm if analyzed from a single image.

According to Nyquist sampling theory [24], frequencies greater than twice the sampling rate will not be resolved, and may furthermore cause aliasing in the digital signal. Typically, aliasing is avoided by the use of an analogue low-pass filter. Inevitably, the sampling process becomes a bandpass filter where frequencies higher than twice the sampling rate are lost. Low frequencies also are lost because wavelengths longer than the field of view can not be represented.

Higher frequencies can be sampled by zooming in during the image acquisition stage, at the cost of losing low frequencies. Lower frequencies can be sampled by zooming out, at the cost of losing high frequencies. Several images can be merged edge-to-edge (forming a mosaic) to increase the sampling of lower frequencies without the loss of higher frequencies. In this manner there is practically no limit to the resolution that can be obtained.

Filtering

Because the sampling grid of an image digitizer is relatively coarse, straight lines often tend to appear stepped in digital form (a phenomenon known as *aliasing*). The stepped line both looks and measures rougher than the straight line that it represents.

The amount of aliasing depends on the angle between the line and the (horizontal) scanning direction of the image digitizing camera. It is most pronounced when this angle is about 22.5° and 67.5°, for the above-specified hardware. For this reason, the shadow to be digitized should be aligned nearly parallel with the scanning axis of the video camera.

A digital smoothing filter, applied along the length of the stepped line after it has been extracted from the digital image, reduces this imposed roughness, but at the same time removes real roughness at high frequencies. Some smoothing appears advantageous, and usually has little detrimental effect.

Digital smoothing is achieved using a five-point Gaussian moving average filter, which recalculates the amplitude of a point on the digitized shadow edge by the following formula:

$$y = 0.06\,y_{i-2} + 0.28\,y_{i-1} + 0.32\,y_i + 0.28\,y_{i+1} + 0.06\,y_{i+2}, \quad (1)$$

where y is the amplitude and i is the position along a profile of constant x spacing. This type of filtering is selected mainly for its tendency to subdue single-pixel spikes or impulses, and edges or steps such as aliasing. However, it also removes any real roughness at that scale, and can only be used if the roughness signal to be measured is of much greater amplitude than the unwanted noise.

Image analysis software

After digitization, the image of the shadow is composed of a matrix of 512 × 480 pixels each with one of 256 grey tones. The image is processed by computer to isolate the shadow-edge and calculate true X–Y coordinates and roughness. The following are the stages of analysis:

1. The scale of the image is calibrated by matching the observed length of the scale bar to its actual length.
2. The angle of incidence Φ, between the illuminating ray and the normal to the rough surface, is calculated as $\tan^{-1}(x/y)$ where y is the known height of sundial post and x is the observed length of its shadow.
3. The grey tone image is converted to a binary (black and white) image by thresholding. The threshold level is adjusted until the shadow becomes black, and the parts of the image not in shadow become white, as in Fig. 1(a).
4. The waveform is isolated by stripping all but the lower edge of the shadow from the thresholded image. Figure 1(a) shows the shadow edge superimposed on the original image, which provides a test of the fidelity of edge isolation.
5. A line-following routine is used to "walk" the length of the isolated shadow waveform, recording its X–Y coordinates.
6. The waveform is smoothed to reduce the aliasing (pixel step effect) introduced by digitization. A five-point Gaussian low-pass (moving average) filter is used.
7. The waveform is converted into a roughness profile of true amplitude by correcting for angles of illumination other than 45°. The observed amplitude of the shadow is multiplied by $\cot \Phi$ where Φ is the angle of illumination as defined above.
8. The centreline of the profile is determined by the least-squares method, minimizing the mean square deviation. If the centreline is not completely horizontal, it and the profile are rotated into a horizontal attitude.
9. Parameters to characterize the roughness are selected, calculated and displayed alongside a graph of the waveform, as in Fig. 1(b).

EVALUATION OF SHADOW PROFILOMETRY

Initial trials at Hemlo Mine

The technique was first evaluated underground in Noranda's Hemlo gold mine in Ontario, Canada. A video camera augmented by still photography was used to record 91 roughness profiles, which were then analyzed. The profiles included three joint sets at five locations and with different base lengths and orientations.

Analysis of variance tests showed a significant difference in the roughness of the three sets, and different roughnesses on the same joint for profiles in different directions.

Sources of error

Potential sources of error include those associated with illumination of the rough surface such as variations in the angle of illumination, intensity of lighting, sensitivity of the camera and reflectivity of the rock (darkness, wetness, dustiness and uniformity of colour of the surface).

A further photographic variable is parallelism between the camera's "horizontal" scan line and the edge of the roughness shadow. With still photography, this is unimportant because the photo print can be rotated when re-scanned in the laboratory. With direct use of a video camera, however, any lack of alignment will introduce aliasing which as noted above, augments the measured roughness.

Variables introduced at the image processing stage include operator subjectivity in picking an appropriate threshold level.

Laboratory investigation of errors

To evaluate the importance of these sources of error, the roughness of a joint face in schist from the Hemlo Mine was measured in the laboratory under a range of conditions.

Errors were evaluated with reference to the roughness profile index R_p, a parameter defined later in this paper. This parameter varies from 1 for a completely smooth surface, to about 1.25 for a very rough rock surface (a value of 1.35 was measured for corrugated cardboard). Errors were determined as a percentage of the maximum expected range (0.25). Similar evaluations were made with reference to the RMS roughness parameter, with similar results that are not reported here.

For each investigation R_p was measured both for the raw data, and for the same data smoothed by a Gaussian digital filter to remove aliasing.

Effect of light intensity, surface speckling and wetness

The Hemlo trials had shown that underexposed profiles give unrealistically high values of R_p. The reason was suspected to be that in poor lighting, dark grains in

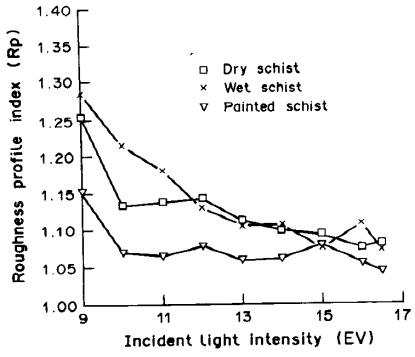

Fig. 3. The effects of varying light intensity, surface wetness and colour on measurements of roughness: an exposure value (EV) of 9 represents a badly underexposed image (−4 F-stops in a photographic metering system) 17 represents a badly overexposed image (equivalent to +4 F-stops). EV = 13 is a correct exposure.

the rock blend with the shadow, adding to its apparent roughness. Confirming this, black dots placed along the length of a shadow on a smooth white surface were found to merge with the digitized shadow-edge, which appeared rougher than it should. The speckled pattern and hence the "artificial roughness" was enhanced when the rock was wet.

To investigate the various lighting effects, a sampling profile was illuminated at 45° and the intensity of a 700 W light source was varied to give images ranging from highly-underexposed to highly-overexposed.

The experiment was repeated three times, first with a dry specimen, then with the surface moistened by spraying with a mist pump, then spray-painted white. The position of the straightedge shadow bar remained unchanged.

Underexposed images were found to give a shadow-edge with poor contrast, difficult to isolate during image processing, tending to merge into the dark rock. The line representing the edge of the shadow undulated more than the true edge of the shadow.

Highly overexposed images gave good contrast but a shadow with a mottled appearance, leading to some difficulty in selecting a threshold level during image processing.

Best results were obtained with proper to moderate overexposure (up to 2 F-stop overexposure in a photographic metering system). Figure 3 shows that the measured roughnesses of dry, wet and white-painted schist all tended to a constant value for light intensities in this range (700–2800 lx, for this particular lighting arrangement). Errors were reduced to acceptable levels of 8 and 3% for unfiltered and filtered profiles, respectively, compared with errors as great as 74% over the entire range of possible illuminations. In practice the entire range need not be considered: the authors have experienced no problem in routinely achieving an exposure value in the correct range.

The experiments confirmed that wet surfaces appear rougher than dry ones, particularly in poor lighting, and that white painted surfaces appear smoothest of all. The smoothness of the painted surface may, however, be partly caused by the film of paint coating the surface.

Angle of incidence of the lighting

A geometrically undistorted roughness profile is created when the angle between the light source and the mean plane of roughness is exactly 45°. As it is inconvenient to ensure 45° illumination in the field, the actual angle of illumination is recorded in the image, and then the shadow trace is corrected (rotated) to give a true profile.

In theory, with this rotation the calculated roughness values should be independent of angle of incidence. In practice, however, some variation has been noted. There are at least four possible causes:

1. With decreasing angles of incidence, the undulation of the trace reduces until its apparent roughness is just a few pixels in amplitude. The amplitude of the roughness signal approaches that of "noise" such as caused by aliasing.
2. With increasing angles of incidence, the edge of the shadow moves away from the shadow bar and the sampling line moves to a slightly different position. This effect is probably not systematic and would give more or less random variations.
3. With increasing angles of incidence, less light is reflected, and the dark shadow does not contrast so strongly with the brightly-lit rock. Dark grains increasingly are confused with the shadow edge, giving greater apparent roughness.
4. At high angles, close to grazing incidence (not investigated in this experiment), the shadows cast by asperities tend to merge with the shadow of the straightedge, making the profile appear rougher.

To quantify this, an experiment was set up where the angle of incidence of the light was varied from 55 to 15° by raising the lamp without moving the specimen or the straightedge. Actual angles were calculated during the image processing stage. The results (Fig. 4) showed an exponential increase in apparent roughness with

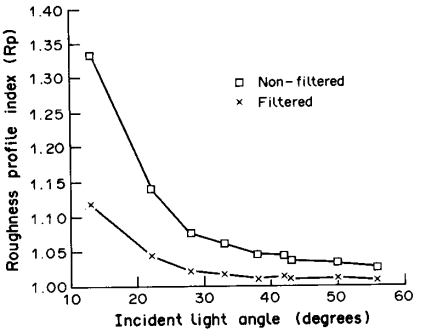

Fig. 4. The effect of angle of illumination on measurements of roughness.

decreasing angles of incidence. The potential error can be summarized as follows:

Angle of light	20–60°	30–60°	40–50°
Original trace (%)	68	22	4
Filtered trace (%)	39	14	1

This leads the authors to conclude that the error resulting from variations in angle of illumination can be held to within about 5% by maintaining this angle at $45 \pm 5°$. Variations of $\pm 10°$ probably will not greatly increase the error, and even larger variations might be tolerated if the image magnification is sufficient to give roughness amplitudes of at least 10 pixels.

Choice of threshold level

To estimate the subjective error when choosing a threshold for shadow-edge isolation, a single shadow profile of the schist surface was analyzed for threshold grey scale intensities in the range 125–170, the complete range possible for that image.

At low threshold values, the shadow edge became discontinuous, whereas at high threshold values, the shadow edge tended to merge into the illuminated rock joint surface. Tests showed that in practice, a threshold in a much narrower range was easily selected, provided that the shadow contrasted well with the rock surface. Only a small range of grey tone thresholds, in this case between 150 and 160, could be chosen, even by an inexperienced operator. Errors for the full range and the more limited and probable range of selected threshold values, with and without filtering, were determined as follows:

	Entire range 125–175	Optimum range 150–160
Original trace (%)	12	2
Filtered trace (%)	3	1

With some care in setting the threshold, the errors from this source were very small.

Measurements on a completely smooth surface

A completely smooth surface should of course register zero roughness. However, on a discretized raster image, straight lines only appear smooth when aligned in the horizontal, vertical and diagonal directions. Any rotation of the line from these four attitudes increases the apparent roughness because the line is stepped as a result of aliasing. Because it is difficult to keep a shadow profile exactly horizontal in the camera's field of view, a slight rotation is always present.

For this experiment, the digitization of a completely smooth trace was simulated by drawing straight lines at various angles from the horizontal using the image analysis system. Figure 5 shows the results. The error in R_p increased sharply for small angles of deviation from both the horizontal and the diagonal. R_p was at a maximum halfway between horizontal and the diagonal. The errors for selected angles were:

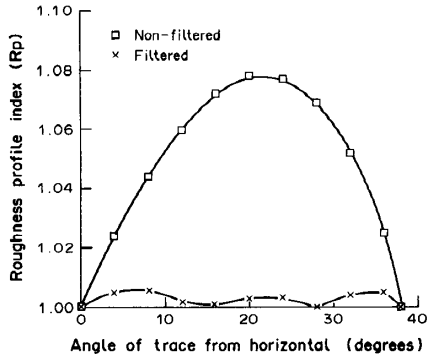

Fig. 5. Check measurements of the roughness of a flat surface.

Angle of the trace from the horizontal	5°	10°	20°
Original trace (%)	13	21	31
Filtered trace (%)	2	2	1

The experiment confirmed an error that was practically eliminated by applying a Gaussian low-pass filter, showing the cause to be aliasing (a pixel effect). However, application of a filter to a relatively smooth joint profile will eliminate not only the noise, but also the real roughness. The solution appears to be firstly to adjust the relative orientations of shadow profile and camera scan line until they are within a few degrees of parallel, and secondly, when measuring relatively smooth surfaces, to ensure sufficient magnification so that a few pixels of aliasing will not be sufficient to mask the true roughness.

Scale effects

Experiments were conducted to investigate scale effects both in the measuring technique, and in the roughnesses of the joint surfaces themselves. The measuring technique was found to be free of scale effects provided that aliasing was rendered insignificant by using an appropriately magnified image. For lack of space in the present publication, joint roughness scale effects will be reported separately.

Reproducibility of a single measurement

Setting the above variables to within the optimum range, the reproducibility of the shadow profile method was tested as follows. Continuous footage was taken with the camcorder of a dry schist joint face with a moderate overexposure. The footage was divided into nine segments by turning the light on and off. Images in each segment were digitized and analyzed identically.

Nine more images were taken with a Vidicon CCTV camera and digitized directly without recording them on video tape. Additionally, images were digitally averaged

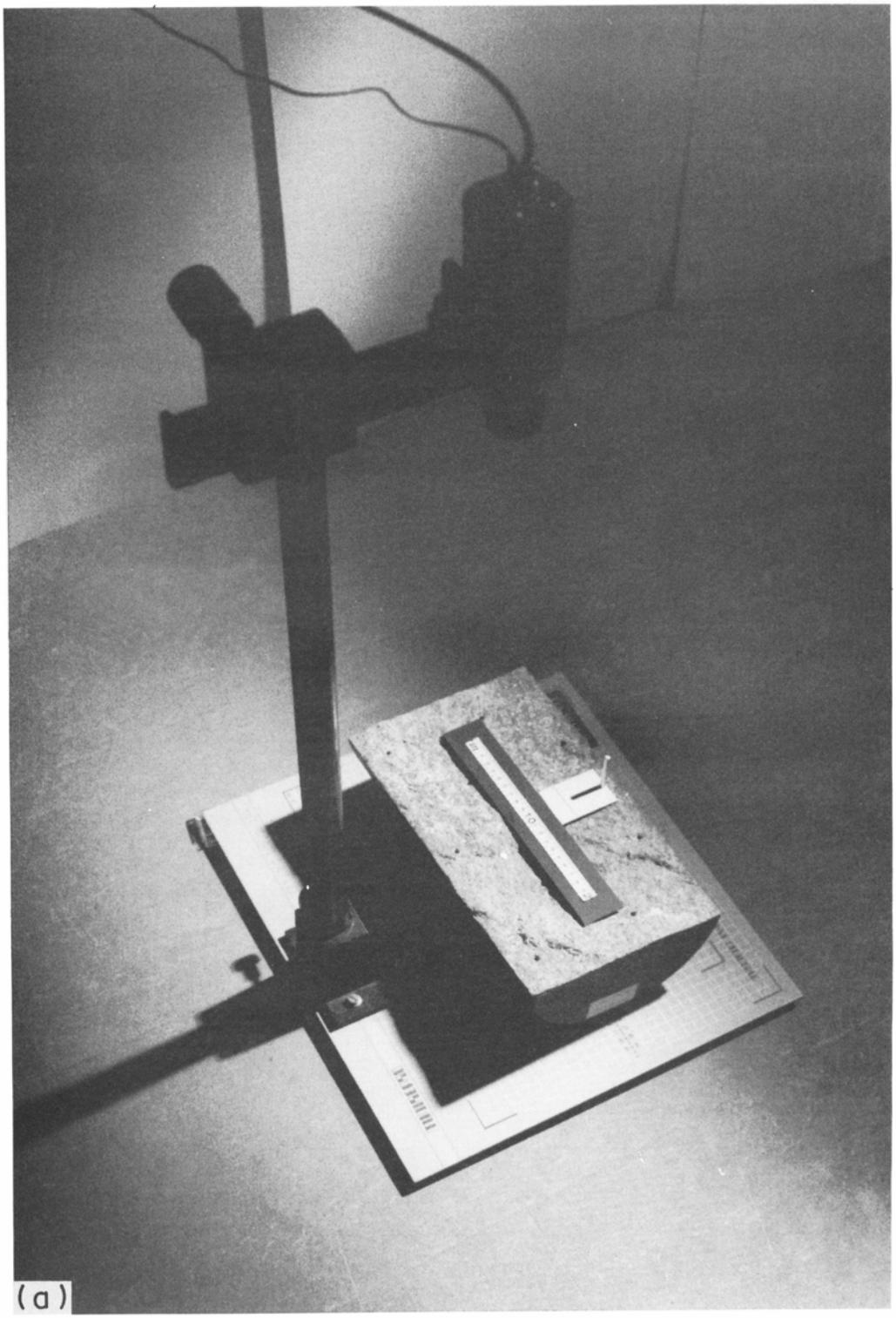

Fig. 6(a)—*Caption overleaf.*

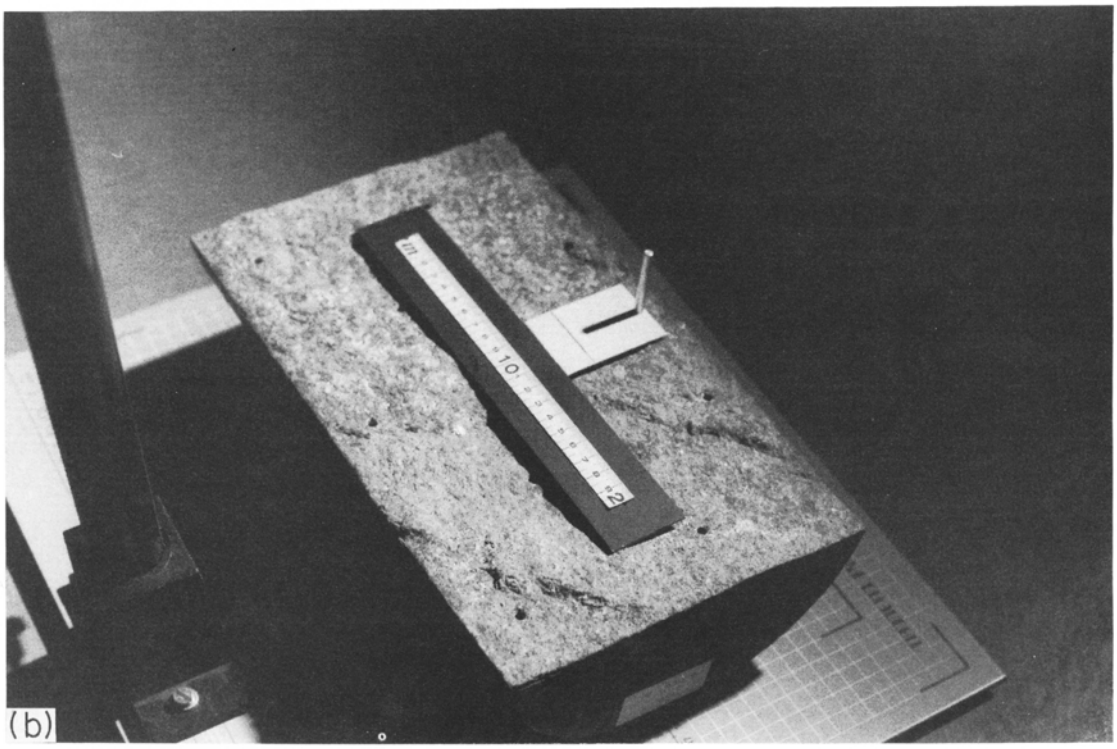

Fig. 6. Laboratory equipment for measuring the roughness of a joint surface cutting a piece of granitic core: (a) camera; and (b) close-up of rock and shadow bar.

for two, four and eight frames. Four tests were done for each level of averaging.

The errors for taped, live and averaged images were determined as follows:

Image type	Taped	Live	Average (2)	Average (4)	Average (8)
Original trace (%)	10	8	4	4	6
Filtered trace (%)	2	2	1	1	2

The results suggest that analyses of live images are marginally less error-prone than taped ones, and that reproducibility can be improved by frame averaging and by filtering. Overall reproducibility of the technique, with reasonable precautions, is estimated as better than $\pm 5\%$ of the full range of roughnesses.

Comparison with mechanical profilometry

A fracture surface running the length of a 325 mm dia piece of core (Fig. 6) was analyzed that had previously been measured by Derek Elsworth and Andrew Piggott at Pennsylvania State University using a mechanical profilometer. The mechanical measurements had, for convenience, been on a 5×5 mm grid. Shadow profile measurements were made along the identical grid lines (spaced 5 mm apart) but at a sampling interval of 0.684 mm along each line.

In an initial comparison, every seventh data point was used in the calculation of roughness, resulting in a sampling interval of 4.79 mm, close to that of the mechanical profilometer. A pair of typical profiles is shown in Fig. 7. The mechanical profile ($R_p = 1.008$) is

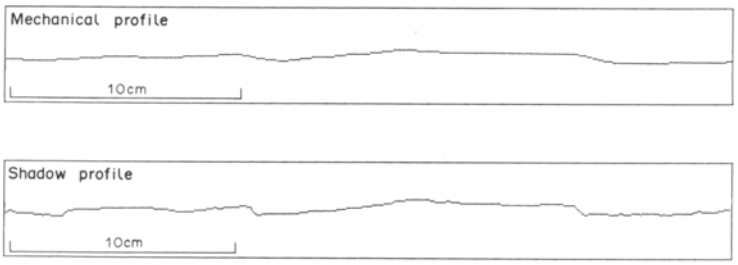

Fig. 7. Comparison of roughness profiles obtained by shadow and mechanical profilometry: the mechanical profilometer (sampling interval 5 mm) tended to suppress the higher roughness frequencies. The sampling interval along the shadow profile was 0.684 mm.

similar to the shadow profile ($R_p = 1.011$), but appears and measures smoother.

Using each data point from the shadow profile resulted in a much greater estimate of roughness ($R_p = 1.019$). This increase in apparent roughness with increased resolution is common in any roughness measure, and is described by Mandelbrot [25] in the classic "How long is the coast of Britain?" problem.

ROUGHNESS PROFILE CHARACTERIZATION

Introduction

The 2-D waveform of a roughness profile is perhaps easier to see and to interpret than a 3-D rough surface, but is still too complex and qualitative to be of much use as it stands. For purposes of predicting the effects of roughness on, say, shear strength, the waveform must be further simplified and characterized in terms of one or several numerical parameters.

Roughness profiles are waveforms, so are analyzed using methods similar to those for processing electrical signals. The methods range from simple measurements of amplitude, wavelength and slope, to more complex stochastic and frequency-domain analyses. The results range from single constants to parameters that are functions of one or several variables.

Amplitude parameters

The scale of geometric irregularities (waves) is sometimes broadly classified into two or more categories, although these are perhaps artificial rather than natural divisions. In rock mechanics, roughness has been categorized as unevenness (small irregularities damaged during shearing) and waviness (larger ones that cause dilation) [20]. In tribology, four orders of roughness have been identified, based on their genesis [14].

The following amplitude measures are described in *American Standards* [13]:

1. The maximum peak to valley roughness height (R_{max}) or waviness height (W) measures the vertical distance between the highest peak and the lowest valley.
2. The levelling depth (R_e) measures the vertical distance between the highest peak and the centreline of the profile.
3. The 10-point height (R_z) measures the average vertical distance between the five highest peaks and five lowest valleys.
4. The average peak-to-valley roughness (R) is the average of all individually measured peak-to-valley heights.

Some of the slightly more sophisticated measures are of the type that determine some statistical amplitude measurement:

1. The Swedish height of irregularities measures the vertical distance containing 90% of the points on the profile, symmetrical about the centreline.
2. Skewness measures the symmetry of the profile line about the centreline.
3. Kurtosis measures the distribution of heights from the centreline.

The root mean square roughness (RMS) is a measure of average deviation from the centreline. In discrete form:

$$\mathrm{RMS} = \left[\frac{1}{n}\sum_{i=1}^{n} y_i^2\right]^{1/2}, \tag{2}$$

where:

n = number of evenly-spaced sampling points,
y = amplitude of sampling point about centreline.

Two variations of this are the centreline average (CLA):

$$\mathrm{CLA} = \frac{1}{n}\sum_{i=1}^{n} |y|_i \tag{3}$$

and the mean square value (MSV) [26]:

$$\mathrm{MSV} = \frac{1}{n}\sum_{i=1}^{n} y_i^2. \tag{4}$$

Wavelength parameters

The following measures of wavelength are also described in *American Standards* [13]:

1. The average spacing (A_r) is the average measured spacing between each adjacent peak.
2. The bearing length ratio (t_p) measures the proportion of the length of the profile that has positive amplitude values above a preselected vertical distance from the centreline.
3. The method of peak counting [27] simply gives a count of the number of peaks per unit length.

Slope parameters

The root mean square of the first derivative of the profile [28] is a single-parameter measure that characterizes a profile based on its average slope:

$$Z_2 = \left[\frac{1}{n\,\mathrm{d}x^2}\sum_{i=1}^{n} (\mathrm{d}y_i)^2\right]^{1/2} \tag{5}$$

where:

n = number of evenly-spaced sampling points,
$\mathrm{d}x$ = distance between points along sampling line,
$\mathrm{d}y$ = distance between points normal to sampling line.

Another parameter is the roughness profile index (R_p), defined as the ratio of the true length of a fracture surface trace to its projected length in the fracture plane [29].

A third slope parameter of roughness, introduced here, is the micro-average i angle (i), defined as:

$$i = \frac{1}{n}\sum_{j=1}^{n} |I_j|, \tag{6}$$

where:

n = number of evenly-spaced sampling points,
I = inclination angle between adjacent points along sampling line.

Myers [28] also introduced the Z_3 parameter, the root mean square of the second derivative of the profile, which is a measure of curvature:

$$Z_3 = \left[\frac{1}{n(\mathrm{d}x_i - \mathrm{d}x_{i-1})^2} \sum_{i=1}^{n} (\mathrm{d}y_i - \mathrm{d}y_{i-1})^2 \right]^{1/2}. \quad (7)$$

The Z_4 parameter, a measure of the directionality of the roughness also defined by Myers [28] is:

$$Z_4 = \frac{\sum (\mathrm{d}x_i)_\mathrm{p} - \sum (\mathrm{d}x_i)_\mathrm{n}}{\sum (\mathrm{d}x_i)_\mathrm{p} + \sum (\mathrm{d}x_i)_\mathrm{n}}, \quad (8)$$

where:

p = positive slope,
n = negative slope.

Power spectra

Roughness can be characterized by spectral density functions, where the profile, as an analogue of a time series, is represented in the frequency domain. Spectral density functions can be represented by Fourier transforms of the original profile data, by Fourier transforms of a previously calculated correlation function, or by bandpass filtering, squaring and averaging of the signal [28].

Stochastic methods

Stochastic methods, in broad terms, incorporate probability density functions for input into analytical models. The amplitude of a roughness profile, for example, can be presented in terms of a mean amplitude component, plus a random amplitude component.

Stochastic methods are based on the assumption that a profile is a random, stationary process. This implies that roughness is independent of position along the length of the profile, and of direction. Thus roughness measured in a small domain is valid for the entire surface [30].

The autocorrelation function (ACF) describes the dependence of amplitude at one location on the amplitude at another location separated by a constant lag distance j:

$$\mathrm{ACF} = \frac{1}{n-j} \sum_{i=1}^{n-j} y_i - y_{i+j}, \quad (9)$$

where:

n = number of evenly spaced sampling points,
y = amplitude of the sampling point about the centreline.

The structure function (SF) [31] has an advantage over the ACF in that it is independent of the mean plane and can be computed over only a portion of the profile without the loss of statistical significance [32]:

$$\mathrm{SF} = \frac{1}{n-j} \sum_{i=1}^{n-j} (y_i - y_{i+j})^2. \quad (10)$$

Fractal dimension

Fractal dimension [25] provides a measure of roughness for profiles that are self-similar *fractal objects*. A profile is self-similar if its shape is the same at all scales of observation. To be represented as a fractal object, roughness therefore should be independent of the scale of observation.

The fractal dimension of a profile can be calculated by counting the number n of "yardsticks" of length r needed to cover the profile. This measurement is repeated for various lengths of r. The fractal dimension D is evaluated by the expression:

$$1 - D = \frac{d(\log_{10} r)}{d(\log_{10} (n \times r))}. \quad (11)$$

The fractal dimension D has a minimum value of 1 for a perfectly smooth profile and a maximum value of less than 2 for an extremely rough undulating profile. In practice it is calculated by plotting r by $n \times r$ on log–log paper and equating the slope to $1 - D$.

Selection criteria

Roughness parameters help convey in a quantitative manner the meaning of terms such as "smooth" and "rough", and allow prediction of characteristics such as shear strength that depend on roughness. Communication among engineers and geologists becomes easier if some measure of standardization can be achieved in selecting which of the many parameters to use. To make a choice, the following factors should be taken into consideration:

(a) the parameters should be insensitive to the techniques of measurement, giving reproducible determinations;
(b) they should faithfully represent the roughness, permitting regeneration of a surface of a similar roughness to the one from which they were derived, given only the parameter values;
(c) they should if possible be simple to visualize, and to relate to meaningful physical characteristics and behaviour;
(d) they should allow prediction of mechanical properties such as shear strength, if possible with use of existing models;
(e) if two or more parameters are selected, they should have a low intercorrelation, i.e. they should represent independent characteristics of roughness to avoid redundancy.

Clearly the selection requires some compromise. The simplest measures, such as the single-parameter ones, record only part of the roughness picture. Measures that best represent the geometry of roughness, such as spectral density, tend to be difficult to visualize and compare

quantitatively. In addition, some of the methods require assumptions of stationarity or scale independence.

The authors have completed a preliminary investigation to determine which parameters are correlated most closely with shear strength, represented by Barton's JRC standard waveforms. As might be expected, the slope parameters have tended to give the closest correlations. These investigations are still in progress.

PREDICTION OF SHEAR STRENGTH

Photoanalysis offers a simple way to predict the shear strength of rock joints, assuming that a correlation can be established between roughness measured directly, and the parameters of a published shear strength criterion.

Patton's shear strength criterion

From Patton's model [4] comes a bilinear peak strength envelope, where roughness, defined as the inclination angle of the asperities on the joint surface, plays an important role for small displacements or low normal stresses:

$$\tau = \sigma_n \tan(\phi_u + i) \tag{12}$$

where:

τ = peak shear strength,
σ_n = normal stress,
ϕ_u = ultimate friction angle,
i = inclination angle of the asperities.

For this idealized model, roughness is related to the inclination angle (i) of the teeth of a sawtooth surface. When applying the model to real rock joints, i is measured as the rise angle of asperities which occur at many different scales. The i angle used is normally the one perceived to have the greatest effect on the shear strength. McMahon [33] recommends measurement of i on asperities whose wavelength is 2% or more of the potential surface of sliding. The Patton model offers a method for "scaling up" laboratory tests to take into account large-scale waviness.

Ladanyi and Archambault's curvilinear model [5] applies to both high and low normal stresses by considering separately the shear stresses on the surface area of intact asperities and on the area of sheared-off asperities. For low normal stress, where roughness plays a role, the model reduces to Patton's linear model as above.

Another roughness parameter, R_p can be used in a Patton type model. Turk and Dearman [34] have suggested that it is related to Patton's i angle by the following equation:

$$i = \cos^{-1}\left[\frac{1}{R_p}\right]. \tag{13}$$

Measurements of i angle can be made by photoanalysis according to whichever definition is preferred. Because of a potential scale dependence, the base length of measurement should be stated. The micro-average i-angle, defined earlier in this paper, could be used for shear strength prediction in a Patton type of model, although it is intended more as an index property that measures the average inclination angle, irrespective of asperity size.

Barton's JRC

Barton's curvilinear shear strength criterion for rock joints [6] is expressed as follows:

$$\tau = \sigma_n \tan[\text{JRC} \log(\text{JCS}/\sigma_n) + \phi_b], \tag{14}$$

where:

τ = peak shear strength,
σ_n = effective normal stress,
JRC = joint roughness coefficient,
JCS = joint wall compressive strength,
ϕ_b = base friction angle.

The name "joint roughness coefficient" is perhaps misleading because JRC is not a measure of roughness geometry, but of shear strength; it is an empirical parameter in a shear strength equation. It cannot be measured directly, but must be estimated either from shear tests on mated rough surfaces, or by visually comparing a rough joint with the standard set of comparator profiles published by Barton and Choubey [15].

Relation between Patton and Barton's models

Patton's and Barton's models for rock joints can be equated to each other, giving:

$$\phi_u + i = \text{JRC} \log(\text{JCS}/\sigma_n) + \phi_b. \tag{15}$$

Assuming further that $\phi_u = \phi_b$ (ultimate friction = base friction angle) gives:

$$i = \text{JRC} \log(\text{JCS}/\sigma_n). \tag{16}$$

In the special case where $\text{JCS}/\sigma_n = 10$, not an unusual situation in nature, the result is that:

$$i = \text{JRC}. \tag{17}$$

Estimation of JRC from published standard profiles

Estimation by visually comparing a joint profile with a set of published standards [15] was found to be unreliable in a test in which two graduate students and three mining engineers participated. The subjects were asked to estimate JRC by visually comparing the standards with 124 profiles obtained by shadow profilometry. The profiles were from three joint sets, sampled *in situ* and by coring, and ranged from 50 to 200 mm in length.

The visual estimates of JRC values in the range 1–18 were in error by an average of ± 3.61 JRC units 95% of the time. Also there were systematic differences between subjects. The spread of average JRC values for all five subjects was 1.4 JRC units.

Avoiding the subjectivity, better results might be obtained by digitizing the standard profiles, measuring their geometric roughness, and correlating one or several roughness parameters with the published JRC values. This was tried by Tse and Cruden [32], who used manual digitization. Our attempts to duplicate their

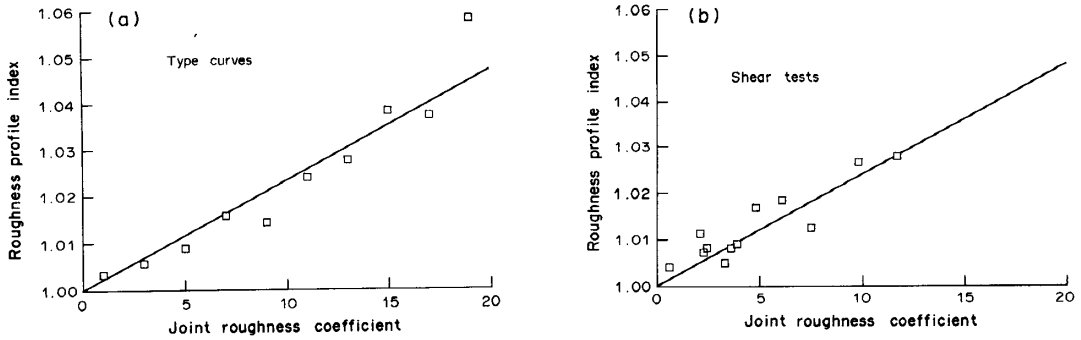

Fig. 8. Correlation between R_p and JRC: (a) obtained by photoanalysis of the type-profiles published by Barton and Choubey [15]; and (b) determined from laboratory tilt and direct shear tests on samples of schist from the Hemlo Mine.

results with a manual digitizing pad were disappointing. The measurements depended on the operator and the steadiness of the hand that traced the profiles.

Greater success was achieved by substituting photoanalysis for manual digitization. The standard profiles were digitized and geometric characteristics computed in the manner described above. Linear regressions between the reported JRC values and the geometric characteristics were then examined. The closest correlation (Pearson's product moment correlation coefficient = 0.984) was obtained with the roughness profile index (R_p). Figure 8(a) shows the plot of JRC vs R_p. From the regression equation, the following relation was found:

$$\text{JRC} = 411\,(R_p - 1). \tag{18}$$

Direct correlation between roughness and JRC

In a further experiment, roughnesses measured by photoanalysis were compared directly with JRC values calculated from shear tests on the same specimens. Cores and blocks 50–300 mm in size were sampled from the Hemlo Mine by personnel of Noranda Mines. Roughness was measured by the shadow profile method six times on each of 12 specimens, which were then subjected to tilt and direct shear tests.

The closest correlation ($R = 0.973$) was obtained with the roughness profile index (R_p). Figure 8(b) shows the plot of JRC vs R_p. The following relation was found by linear regression:

$$\text{JRC} = 401\,(R_p - 1). \tag{19}$$

This compares quite closely with equation (18) given above, derived from the published standard profiles.

CONCLUSIONS

Shadow profilometry has been evaluated both in a mining and a laboratory context. It is a straightforward and reliable method. Using this and related techniques of photoanalysis, a survey of a mine by video camera can provide much of the information on jointing needed for rock mass classification and analysis of stability.

Overall reproducibility, with reasonable precautions, is estimated as better than $\pm 5\%$ of the full range of roughnesses, and can be improved by magnification, by frame averaging and by filtering. Lighting should be sufficient, and ideally the angle of illumination should be $45 \pm 5°$. Image magnification should be sufficient to give roughness amplitudes of at least 10 pixels, and the profile should fill the screen. Analyses of live images are marginally less error-prone than of taped ones.

Roughness parameters help convey the meaning of "smooth" and "rough", and permit quantitative predictions of such properties as shear strength. Alternatives range from simple measurements of amplitude, wavelength and slope, to more complex stochastic and frequency domain analyses. Few of these are in common use in rock mechanics, and the ones most used are not necessarily the best for characterizing a joint or for representing its mechanical or hydraulic behaviour.

Estimation of joint roughness by visually comparing a joint profile with a set of published standards was found to be unreliable. Visual estimates of JRC values in the range 1–18 were in error by an average of ± 3.61 JRC units 95% of the time. Greater success was achieved using $\text{JRC} = 411\ (R_p - 1)$, where R_p is measured by photoanalysis. A similar relation was found by correlating JRC estimated by photoanalysis with direct measurements of shear strength.

Acknowledgements—The research described in this paper has been sponsored by the Centre de Téchnologie Noranda, who also obtained and tested samples of rock from the Noranda Mines. The authors would like to thank their colleagues in the mining industry, particularly Mr Jacques Nantel, Will Bawden, Paul Germain and Doug Milne for their cooperation and for releasing the test results for publication.

The authors would like to thank also Professor Derek Elsworth and Andrew Piggott of Pennsylvania State University for supplying the granite core sample and the mechanical profilometry results. Participants in the research have included students at the University of Waterloo working on other applications of photoanalysis. Jose Ibarra developed improved lighting with the assistance of Professor Eastman. Tony Butler assisted in the experimentation, both in the laboratory and underground.

Accepted for publication 6 December 1989.

REFERENCES

1. Franklin J. A. and Maerz N. H. Digital photoanalysis of rock jointing. *In situ* testing and field behaviour. *Can. Geotech. Conf.*, pp. 11–20 (1986).
2. Maerz N. H., Franklin J. A., Rothenburg L. and Coursen D. L. Measurement of rock fragmentation by digital photoanalysis. *Proc. 6th Int. Congr. Rock Mech.*, Montreal, Canada, Vol. 1, pp. 687–692. Balkema, Rotterdam (1987).
3. Franklin J. A., Maerz N. H. and Bennett C. P. Rock mass characterization using photoanalysis. *Int. J. Min. Geol. Engng* **6,** 97–112 (1988).
4. Patton F. D. Multiple modes of shear failure in rock. *Proc. 1st Int. Congr. Rock Mech.*, Lisbon, Portugal, Vol. 1, pp. 509–513. Laboratório Nacional De Engenharia Civil, Lisbon, Portugal (1966).
5. Ladanyi B. and Archambault G. Simulation of shear behaviour of a jointed rock mass. Rock mechanics in theory and practice. *Proc. 11th U.S. Symp. Rock Mech.*, pp. 105–125 (1969).
6. Barton N. Review of a new shear-strength criterion for rock joints. *Engng Geol.* **7,** 287–332 (1973).
7. Swan G. Determination of stiffness and other joint properties from roughness measurements. *Rock Mech.* **16,** 16–38 (1983).
8. Bandis S. C., Lumsden A. C. and Barton N. R. Fundamentals of rock joint deformation. *Int. J. Rock Mech. Min. Sci. & Geomech. Abstr.* **18,** 1–21 (1985).
9. Swan G. and Zongqi S. Prediction of shear behaviour of joints using profiles. *Rock Mech.* **18,** 183–212 (1985).
10. Barton N., Bandis S. and Bakhtar K. Strength, deformability and conductivity coupling of rock joints. *Int. J. Rock Mech. Min. Sci. & Geomech. Abstr.* **22,** 121–141 (1985).
11. Elsworth D. and Goodman R. E. Characterization of rock fissure hydraulic conductivity using idealized wall roughness profiles. *Int. J. Rock Mech. Min. Sci. & Geomech. Abstr.* **23,** 233–243 (1986).
12. Halling J. *Introduction to Tribology*. Wykeham, London (1976).
13. ASME. *American National Standard, Surface Texture, Surface Roughness, Waviness and Lay*. American Society of Mechanical Engineers, New York (1978).
14. Thomas T. R. *Rough Surfaces*. Longman, London (1982).
15. Barton N. and Choubey V. The shear strength of rock joints in theory and in practice. *Rock Mech.* **10,** 1–54 (1977).
16. Zaniewski J. P. and Moser L. Root-mean-square vertical acceleration as a summary roughness statistic. *Measuring Road Roughness and its Effects on User Cost and Comfort. ASTM Special Technical Publication 884* (T. D. Gillespie and M. Sayers, Eds), pp. 3–24 (1985).
17. Schmaltz G. *Technische Oberflächenkunde*. Springer, Berlin (1936).
18. Hung Yau Y. Displacement and strain measurement. *Speckle Metrology*, pp. 51–72. Academic Press, New York (1978).
19. Olsen W. S. and Adams R. M. A laser profilometer. *J. Geophys. Res.* **75,** 2185–2187 (1970).
20. ISRM Commission on Testing Methods. The quantitative description of discontinuities in rock masses. *Rock Characterization, Testing and Monitoring—ISRM Suggested Methods*, pp. 3–52. Pergamon Press, Oxford (1981).
21. Fecker E. and Rengers N. Measurement of large scale roughness of rock planes by means of profilograph and geological compass. Rock fracture. *Proc. Symp. Int. Soc. Rock Mech.*, Nancy, France, pp. 1–18 (1971).
22. Weissbach G. A new method for the determination of the roughness of rock joints in the laboratory. *Int. J. Rock Mech. Min. Sci. & Geomech. Abstr.* **15,** 131–133 (1978).
23. Wickens E. H. and Barton N. R. Application of photogrammetry to the stability of excavated rock slopes. *Photogram. Record* **7,** 46–54 (1971).
24. Oppenheim A. V. and Schafer R. W. *Digital Signal Processing*. Prentice Hall, Englewood Cliffs, New Jersey (1975).
25. Mandelbrot B. *The Fractal Geometry of Nature*. Freeman, San Francisco (1982).
26. Bendat J. S. and Piersol A. G. *Random Data. Analysis and Measurement Procedures*. Wiley, New York (1985).
27. Society of Automative Engineers (U.S.A.). Surface texture measurement of cold rolled steel. *SAE Recommended Practice. SAE Handbook*, Vol. 1, pp. 9.01–9.03 (1986).
28. Myers M. O. Characterization of surface roughness. *Wear* **5,** 182–189 (1962).
29. El-Soudani S. M. Profilometric analysis of fractures. *Metallography* **11,** 247–336 (1978).
30. Reeves M. J. Rock surface roughness and frictional strength. *Int. J. Rock Mech. Min. Sci. & Geomech. Abstr.* **22,** 429–442 (1985).
31. Sayles R. S. and Thomas T. R. The spatial representation of surface roughness by means of the structure function: a practical alternative to correlation. *Wear* **42,** 263–276 (1977).
32. Tse R. and Cruden D. M. Estimating joint roughness coefficients. *Int. J. Rock Mech. Min. Sci. & Geomech. Abstr.* **16,** 303–307 (1979).
33. McMahon B. K. Some practical considerations for the estimation of shear strength of joints and other discontinuities. *Proc. Int. Symp. on Fundamentals of Rock Joints*, Björkliden, pp. 475–485 (1985).
34. Turk N. and Dearman W. R. Investigation of some rock joint properties: roughness angle determination and joint closure. *Proc. Int. Symp. Fundamentals of Rock Joints*, Björkliden, pp. 197–204 (1985).